Journal of Magnetic Resonance 197 (2009) 135–144

Contents lists available at ScienceDirect

Journal of Magnetic Resonance

journal homepage: www.elsevier.com/locate/jmr

A low-E magic angle spinning probe for biological solid state NMR at 750 MHz

Seth A. McNeill [b], Peter L. Gor'kov [c], Kiran Shetty [c], William W. Brey [c], Joanna R. Long [a,*]

[a] Department of Biochemistry and Molecular Biology and McKnight Brain Institute, University of Florida, Box 100245, Gainesville, FL 32610-0245, USA
[b] Department of Electrical and Computer Engineering, University of Florida, FL 32611, USA
[c] National High Magnetic Field Laboratory, Tallahassee, FL 32310, USA

ARTICLE INFO

Article history:
Received 9 August 2008
Revised 2 December 2008
Available online 14 December 2008

Keywords:
Solid state NMR
Magic angle spinning
Membrane proteins
Probe design
Loop gap resonator
Low-E
Rf heating

ABSTRACT

Crossed-coil NMR probes are a useful tool for reducing sample heating for biological solid state NMR. In a crossed-coil probe, the higher frequency ^{1}H field, which is the primary source of sample heating in conventional probes, is produced by a separate low-inductance resonator. Because a smaller driving voltage is required, the electric field across the sample and the resultant heating is reduced. In this work we describe the development of a magic angle spinning (MAS) solid state NMR probe utilizing a dual resonator. This dual resonator approach, referred to as "low-E," was originally developed to reduce heating in samples of mechanically aligned membranes. The study of inherently dilute systems, such as proteins in lipid bilayers, via MAS techniques requires large sample volumes at high field to obtain spectra with adequate signal-to-noise ratio under physiologically relevant conditions. With the low-E approach, we are able to obtain homogeneous and sufficiently strong radiofrequency fields for both ^{1}H and ^{13}C frequencies in a 4 mm probe with a ^{1}H frequency of 750 MHz. The performance of the probe using windowless dipolar recoupling sequences is demonstrated on model compounds as well as membrane-embedded peptides.

1. Introduction

Performing NMR experiments at high magnetic fields increases their applicability to systems that are resolution or sensitivity limited. Polarization enhancement estimates suggest the increase in signal-to-noise (S/N) should be on the order of $B_0^{7/4}$, decreasing acquisition times by a factor of $B_0^{7/2}$. With the advent of stable high field instruments with proton frequencies of 700 to over 900 MHz, the application of solid state NMR (ssNMR) spectroscopy to a wide variety of biomolecular systems has become increasingly feasible. However, realizing these sensitivity gains for a variety of samples, nuclei, and pulsed experiments is not straightforward since the increase in signal is accompanied by an increase in the isotropic and anisotropic chemical shifts. This results in increased spectral widths requiring the generation of more powerful B_1 fields to excite all frequencies of interest. Additionally, as at lower magnetic fields, many ssNMR experiments require proton decoupling with rf field strengths above $(\omega_1/2\pi) = 100$ kHz on the proton channel for optimal resolution.

With traditional ssNMR probe circuits utilizing multiply-resonant solenoidal coils, achieving efficient and homogeneous B_1 fields is complicated by the electrical length of the sample coil at high proton frequency approaching a quarter of the rf wavelength [1,2]. The study of biomolecules under physiologically relevant conditions substantially alters the probe performance by loading the coil with samples containing high salt concentrations. Creating stronger B_1 fields also creates stronger electric (E) fields within the sample leading to more heating and, ultimately, sample degradation. The generation of E fields and their contributions to sample heating in ssNMR spectroscopy have been extensively studied in recent years [3–14]. This heating can be overcome by cooling samples down to where the heating does not disrupt the system [3], but often this means cooling the samples well below biologically relevant temperatures which can alter protein conformation or remove the molecular dynamics of interest. Lowering the conductivity of the samples is another method of reducing heating [14]. This is possible for some samples, but again may lead away from biologically relevant conditions. Common spectroscopic approaches to minimizing sample heating include the use of very low duty cycles and utilizing very small coils, with a subsequent reduction in scans per unit time and sample volume, respectively, leading to poorer S/N and/or longer acquisition times, particularly for concentration-limited samples.

More recently, probe design efforts have focused on the more fundamental issue of modifying the coil design by reducing inductance and/or adding shielding to reduce sample heating. Traditional multinuclear ssNMR probe designs employ a single, multiply-resonant solenoid as this maximizes the filling factor for the various frequencies and (when wavelength effects can be

* Corresponding author. Fax: +1 352 392 3422.
E-mail address: jrlong@mbi.ufl.edu (J.R. Long).

1090-7807/$ - see front matter © 2008 Elsevier Inc. All rights reserved.
doi:10.1016/j.jmr.2008.12.008

neglected) helps ensure rf overlap. Several clever modifications to the solenoid have been proposed to reduce heating while preserving as much as possible the efficiency of both high and low-frequency channels. These designs also allow commercial probe suppliers to continue to use their well-developed multichannel matching networks. Scroll coils [15] offer a robust solution to the problem of sample heating as they have a lower inductance than solenoids and their geometry creates a built-in Faraday shield for the *E* field since the inner turns shield the sample from the *E* field generated by the outer turns [4]. Both these factors reduce sample heating and improve stability and performance on the proton channel. The ^{1}H efficiency of scroll coils with lossy samples can surpass that of solenoids. However, scroll coils are less efficient than solenoidal coils at lower frequencies due to their low-inductance and low Q [4]. Scroll coils also present challenges due to temperature dependant tuning changes inherent to the large capacitance between turns [7,11]. This capacitance also limits the available sample volume [9]. The Z-coil, consisting of a central loop with two spiral coils on the ends of the loop [10], lowers sample heating by more than an order of magnitude relative to a solenoidal coil and has an rf efficiency that is independent of sample conductivity. However, unlike the scroll, the rf efficiency of the Z-coil with a lossy sample is just comparable to that of the solenoid, and there is also a penalty in sensitivity and efficiency at the lower frequencies. Most recently, Krahn and co-workers have shown that heating can be reduced by inserting a conductive shield between the sample and the solenoid [13]. Precise manufacturing of the shield led to an effective decrease in heating at a modest cost in sensitivity due to the decrease in sample filling factor compared to an unshielded solenoid. However, the close proximity of the shield to the sample coil can be expected to the limit the voltages, and hence the achievable B_1, for larger sample volumes. These three single-coil alternatives to the solenoid have been shown to reduce heating at some cost to rf efficiency. While the gains in rf and temperature stability certainly outweigh the loss in sensitivity for lossy samples, an alternative approach which does not compromise the sensitivity and efficiency of the lower frequencies would be attractive, particularly since the bulk of biological ssNMR experiments rely on direct detection of low gamma nuclei due to proton resolution limitations at slow to intermediate magic angle spinning speeds.

One such solution to achieve the desired rf performance at the proton frequency and simultaneously reduce sample heating is to use separate coils for the low and high frequencies. There are several benefits to this design: using two coils allows the individual circuits and coils to be optimized for each frequency range; having one coil inside the other allows the inner coil to act as a partial Faraday shield for the outer coil; the rf fields generated by the two coils can be designed to be orthogonal, which increases channel isolation and therefore efficiency; and, when the coil assembly is rotated for magic angle applications, the use of orthogonal coils results in a compromised rf field on only one coil.

An advantageous approach for using crossed coils in MAS probes is to place a low-inductance, segmented ^{1}H saddle coil inside a solenoid tuned for the lower frequency channel [7]. With this configuration, the ^{1}H coil shields the sample from some of the *E* fields created by the inductance of the solenoid. The inverse configuration, in which the low-frequency sensitivity is improved by placing a solenoid within a loop gap resonator (LGR), has been used effectively to reduce heating in large volume static probes [9] and is the focus of this project. The LGR is a coil geometry which works well at proton frequencies due to its low-inductance, lower *E* fields, and short electrical length; LGRs have been used extensively in EPR for high frequency applications [16] as well as in MRI [17]. Previously, we have shown that they also work well for high field ssNMR applications when combined with an orthogonal inner solenoid for the lower gamma nuclei [9], a design we have christened "low-E" due to its favorable mitigation of *E* fields within the sample space. In such designs, the sample is placed within a solenoidal coil to maximize sensitivity and homogeneity for the low-frequency channel; an LGR optimized for the proton channel is orthogonal to and surrounds the solenoid. In this configuration, the solenoid further lowers the *E* field by acting as a partial Faraday shield between the sample and the LGR. The outer ^{1}H resonator is slit strategically to cancel low-frequency eddy currents which would otherwise reduce the efficiency of the inner coil. The loss of filling factor for the proton channel in a crossed coil setup like this is largely made up for by the improved efficiency of the single-frequency ^{1}H matching network. And since the solenoid is not called upon to produce a ^{1}H field, its length and number of turns can be increased to improve sensitivity. For a MAS probe, the fact that the rf field of the LGR can be made orthogonal to the polarizing magnetic field B_0 further improves ^{1}H efficiency relative to a multiply-tuned solenoid.

An additional benefit of the LGR ^{1}H coil is that its homogeneity is excellent. The high B_1 homogeneity on both channels of the ^{1}H LGR/^{13}C solenoid configuration is of critical importance for the application of cross-polarization (CP) and multipulse experiments to samples which are concentration-limited. In multipulse recoupling experiments, especially long windowless experiments, the accumulation of phase errors from different parts of the sample nutating at different rates leads to reduced excitation efficiencies and phase errors in the resulting signals. The increased homogeneity of the LGR at the proton frequency and the solenoidal coil at lower frequencies can increase the efficiency and final signal strength of multipulse experiments, particularly experiments which utilize double quantum filtering.

In considering concentration-limited samples, the ^{1}H LGR/^{13}C solenoid configuration allows reasonably straightforward scaling of the sample volume even at high frequencies. For samples which are inherently dilute (i.e. membrane proteins in lipid vesicles or proteins adsorbed on to solid substrates), it is often preferable to use larger sample volumes. This is because sensitivity per unit volume scales as $\sim(1/d)$ with respect to the rotor diameter while full rotor sensitivity scales as d^2, so a larger sample diameter presents significant advantages for concentration-limited samples if sufficient rf strength and homogeneity can be achieved [18].

In this paper we present the design and characterization of a ssNMR magic angle spinning (MAS) probe that utilizes a ^{1}H LGR placed orthogonally to a ^{13}C solenoid implemented on an NMR system with a 17.6 T magnet (750 MHz ^{1}H frequency). The design was optimized for intrinsically dilute samples by utilizing a 4 mm rotor. The use of two separate coils allowed us to significantly increase both the length and number of turns in the solenoidal coil, making highly homogeneous B_1 fields achievable even with the increased volume of the coil.

2. Probe design and performance characterization

2.1. Sample coil assembly and integration into a MAS stator

The probe design described and characterized in this paper is an adaptation of a previously reported static low-E probe [9]. The coil assembly consists of two rf coils which are orthogonal to each other. The outer coil is a rectangular LGR tuned for the ^{1}H circuit and the inner coil is a solenoidal coil for the low gamma nucleus. In previous work this assembly was optimized for PISEMA experiments on static, oriented membrane-embedded protein samples. For the present MAS application, the coil assembly (Fig. 1a) was modified so that it could be integrated into a 4 mm MAS stator (model AMP4023-001, Revolution NMR, Inc., Fort Collins, CO) with a top spinning speed of 18 kHz. In MAS implementation of low-E

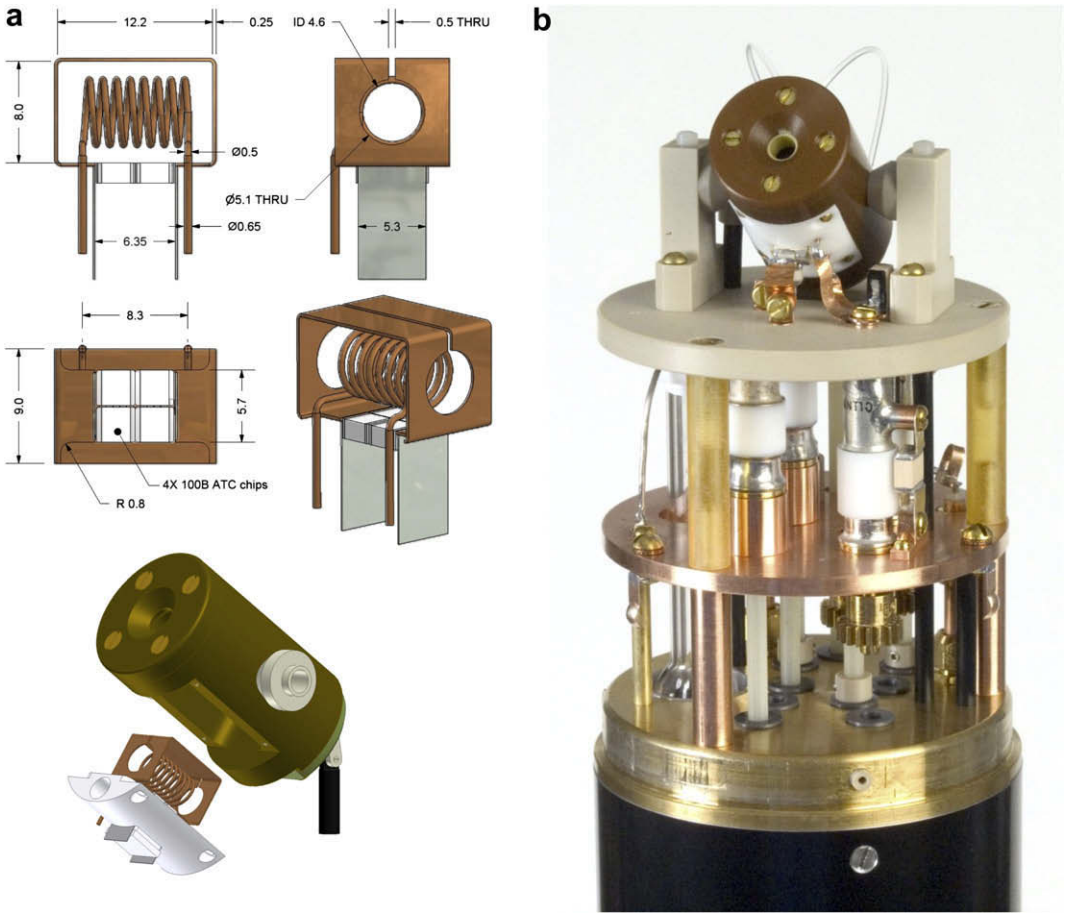

Fig. 1. (a) Physical dimensions of the coils (in millimeters) and their integration into a MAS stator using a Teflon coil centering platform; (b) photograph of the probe head. The Teflon coil platform and two pairs of leads can be seen at the bottom of the stator. The observe solenoid is made using a variable pitch winding which is not reflected in the drawing.

coils, the sensitivity of the detection channel benefits from a stator design where MAS bearings are placed further apart as this provides space for additional turns in the observe solenoid. The coil cavity available in the stator measures 11 × 12 mm in cross-section and 20 mm in length, which is substantially longer than the 12.7 mm length of our coil assembly. This stator is compatible with standard Varian 4.0 mm Pencil style rotors (Revolution NMR p/n AMP4088-001 or Varian p/n MSPA003006). The exact physical dimensions for both coils are provided in Fig. 1a. Regulation of sample temperature is accomplished by VT gas delivered through the side of the stator. A photograph of the fully assembled probe head is shown in Fig. 1b.

The loop gap resonator was fabricated by forming a 0.25 mm thick, 9.0 mm wide copper strip around a 12.2 × 8 mm rectangular block. The ends of the strip were terminated with non-magnetic chip capacitors (100B series, American Technical Ceramics) to complete the LGR. The resonator was attached to the ^{1}H matching network using low-inductance leads threaded through a Teflon platform that centers the coil assembly in the stator housing (Fig. 1). The inner, low gamma coil is an 8-turn 4.6 mm ID × 8.3 mm long cylindrical solenoid. The solenoid was made from 0.6 mm round copper wire (American Wire Gauge #22). Locating the low-frequency coil closest to the sample maximizes sensitivity for direct detection. The homogeneity of the B_1 field was improved by using variable spacing between the coil windings. The solenoid leads were also threaded through the Teflon platform which centers the coil with respect to the LGR and the MAS stator.

2.2. Rf matching network

The double-tuned X–^{1}H matching network implemented in our MAS probe is shown schematically in Fig. 2. The design and performance of this rf circuit has been thoroughly described [9]. For the purposes of the applications described below, the detection channel was tuned to ^{13}C. It can be re-tuned to any other low gamma nuclei by exchanging capacitors C_{7A} and C_8. Variable capacitors C_5, C_6, and C_7 in the low-frequency circuit are 1–10 pF trimmers (NMNT10-6, Voltronics Corp., Denville, NJ). In the proton channel, C_1 is a 1 to 6 pF trimmer (Voltronics NMQM6G), C_2 and C_3 are 0.3–3 pF trimmers (RP-VC3-6, Polyflon Co. Norwalk, CT). Non-magnetic fixed capacitors employed in the proton matching network are Voltronics 11 series chips. In the low-frequency channel, we used non-magnetic 100C series chips from American Technical Ceramics, Huntington Station, NY.

The chip capacitor values for the proton LGR (L_0–C_0) had to be chosen to resonate it slightly above the Larmor frequency. This self resonance frequency is affected by the dielectric material of the stator and the coil platform which are in close proximity. A small loop was inserted through a side hole in the stator to pickup the resonant frequency f_0 of the entire stator assembly. Chip values (C_0) were chosen to place f_0 between 780 and 790 MHz.

2.3. Power efficiency and homogeneity of rf fields

The low-E resonator MAS probe was fully characterized via NMR experiments using a 750 MHz Bruker AV2 system with an

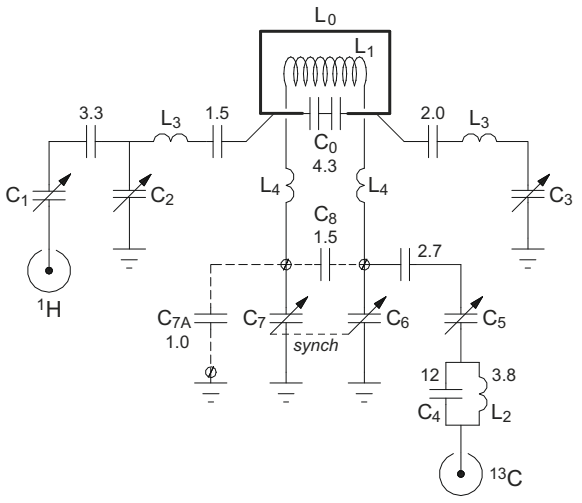

Fig. 2. Schematics of the double-tuned rf matching network. L_0–C_0 forms the ^{1}H loop gap resonator with the detection solenoid inside (L_1). Inductors L_3 and L_4 (5–10 nH each) represent flexible leads connecting sample coils to the ^{1}H and ^{13}C circuits. C_1, C_2, and C_3 are variable capacitors for, respectively, matching, balancing, and tuning the ^{1}H LGR. In the low-frequency channel, C_5 is used for matching while C_6 and C_7 tuning capacitors are connected to a single tuning rod via a gear mechanism. Retuning to different observe nuclei (e.g. ^{15}N) is done by replacing a tuning chip, C_8, and a balancing chip, C_{7A}. A low-voltage ^{1}H rejection trap, L_2–C_4, is placed at the entry of the ^{13}C rf cable.

89 mm bore magnet and a CPC MRI Plus model 19T300 ^{1}H amplifier. The power going into the probe was measured using a directional coupler and an rf power meter (Agilent E4416A meter with an E9323A power sensor). Adamantane (Acros Organics) was used for direct observation of the ^{13}C and ^{1}H resonances for B_1 field and homogeneity measurements since it is a low-loss material and its dipolar couplings are inherently small due to molecular motion and can be removed to first order by MAS at moderate rates. It was also used for calibrating chemical shifts and lineshape measurements. For restricted volume measurements, Kel-F spacers were used to reduce the sample length and to center the sample within the coils. ^{1}H and ^{13}C nutation experiments utilized a variable length single pulse on the observe channel and, for ^{13}C experiments, CW proton decoupling (83 kHz) was applied during acquisition. ^{13}C homogeneity was determined by irradiating and monitoring the carbon resonance at 38.48 ppm; ^{1}H homogeneity was determined by irradiating and monitoring the unresolved proton resonances at an average position of 2.6 ppm.

The maximum ^{1}H power available on the spectrometer is 220 W, which is below the power limit of the probe. With our limited available power, the maximum ^{1}H decoupling field is achieved by bypassing the duplexer and connecting the amplifier output directly to the probe, and this is the setup we typically use in ssNMR experiments. To measure maximum ^{1}H nutation rates achievable by this setup using NMR, we prepared a sample of chloroform sealed in a 1 mm capillary with 5 min epoxy. The capillary was inserted inside a thick-walled rotor along with ground KBr to stabilize the spinning at ~1 kHz. The ^{1}H nutation rate was then measured via indirect detection.

B_1 homogeneity measurements as a function of adamantane sample length are shown in Fig. 3a. Homogeneity is reported as the ratio of the signal intensities after 810° and 90° pulses (810°/90°). Rf field strengths ($\omega_1/2\pi$) were measured to be 104 kHz at 220 W of input power for ^{1}H (750.2 MHz) and 72 kHz at 75 W of input power for ^{13}C (118.6 MHz). As expected, the LGR coil for the proton channel, the increased number of turns in the solenoidal coil, and restricting the sample length to within the coils leads

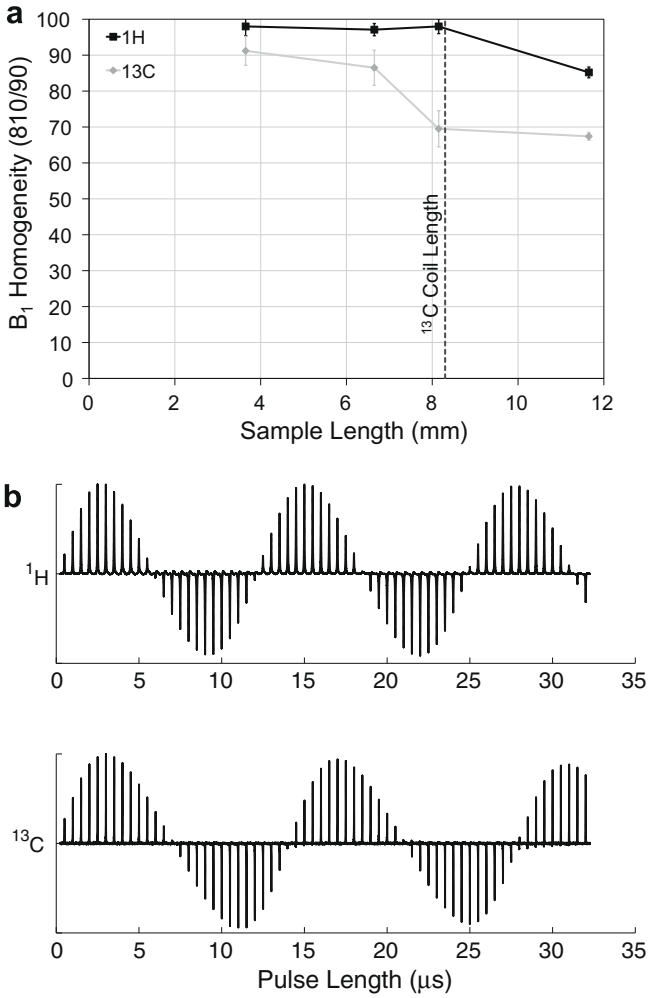

Fig. 3. (a) B_1 homogeneity characteristics for the ^{1}H (black squares) and ^{13}C (gray diamonds) channels as a function of sample length. The ^{13}C solenoidal coil length, 8.3 mm, is indicated by the dashed vertical line. As expected, homogeneity is high and improves when the sample is confined within the coil. (b) Nutation profiles for the ^{1}H (top) and ^{13}C (bottom) channels collected using a 6.7 mm long adamantane sample. Each peak corresponds to the monitored resonance as a function of the pulse length in 0.5 μs increments.

to enhanced B_1 homogeneity at both low and high frequencies. Example nutation profiles for both ^{1}H and ^{13}C can be seen in Fig. 3b. The length of sample in Fig. 3b is 81% of the length of the solenoid. Isolation between probe channels was measured using a HP8752C Vector Network Analyzer (Hewlett Packard). Without external filters, the isolation achieved between the ^{13}C and ^{1}H ports is 45 dB at the ^{1}H frequency and 24 dB at the ^{13}C frequency.

Placement of the ^{1}H loop gap resonator as the outer coil leads in principle to less efficient performance on the high frequency channel, but this compromise is offset by orienting the resonator orthogonal to B_0 and by the high rf homogeneity of the LGR. By choosing this geometry, the ^{1}H B_1 field in the x–y plane is not attenuated by rotation of the coil assembly from a static orientation orthogonal to the external magnetic field to an orientation in which the solenoidal coil axis is at the magic angle. More importantly, the placement of the solenoidal coil inside the assembly improves the filling factor on the observe channel. This helps to offset the loss of B_1 field in the solenoid due to its magic angle orientation. Because the length of the solenoid is not limited by ^{1}H wavelength effects, we are able to utilize an 8-turn solenoid, which further improves the performance of the ^{13}C channel relative to multiply-tuned solenoids containing fewer turns.

2.4. Power handling and stability

The probe's power handling capabilities were bench tested to determine if long, high-power pulses led to either arcing or detuning of the resonant circuits. No arcing was observed during 80 ms long pulses in the ^{1}H channel at powers exceeding 280 W, which corresponds to $(\omega_1/2\pi) \approx 117$ kHz. However, the first implementation of the probe exhibited detuning of the ^{1}H resonance by as much as 0.9 MHz once the decoupling pulse length exceeded 20 ms. The chip capacitors in the ^{1}H LGR are heated up by the high current needed to produce strong decoupling fields, and this can lead to small changes in capacitor values. This problem was narrowed down to a lack of cooling mechanism for these chips. To correct it, a channel was cut in the Teflon platform underneath the chip capacitors, allowing the gases circulating inside the sample compartment to flow around the chips and cool them on all four sides. This measure significantly decreased detuning of the ^{1}H channel to a much smaller, comfortable level, which would not require tuning adjustments during NMR experiments. A subsequent test has shown that high-power detuning in the ^{1}H channel can be eliminated if the 100B series chip capacitors in the LGR are replaced by their temperature-compensated NP0 counterparts, such as non-magnetic version of 700B series. The ^{13}C channel was stable under high-power conditions with pulses up to 20 ms in length at powers exceeding 75 W ($\omega_1/2\pi \approx 72$ kHz) and 5 ms long pulses at 117 W ($\omega_1/2\pi \approx 90$ kHz).

2.5. Shimming

The probe shims adequately without spending extensive time. The ^{13}C full width at half height for adamantane is 9 Hz at a sample length of 3.7 mm; the 0.55% linewidth is 83 Hz. For the full rotor length, 11.7 mm, the half height linewidth is 11 Hz. A small foot is observed in the ^{13}C signal which is similar to inhomogeneous broadening we have observed in a commercial XC4 probe from Doty Scientific. Our lineshape would likely be improved by using zero susceptibility wire in the solenoid which is closest to the sample, but the opportunity to test this hypothesis has not arisen. Another source of inhomogeneity may be the capacitors for the ^{1}H coil. However, they are more physically distant from the sample, so we expect their contribution to the observed broadening to be less, relative to the ^{13}C coil wire.

3. Measurements of sample heating

3.1. Rf-induced heating

To characterize rf performance with typical biological samples, test samples containing either D_2O or 0.15 M NaCl in D_2O were prepared. Experiments were performed using the full rotor volume (57 μL for a thick-walled rotor) as well as more restricted sample lengths. Rotors were sealed with PTFE tape gaskets and sample lengths were varied using Kel-F spacers.

To measure rf-induced heating, aqueous samples described above were doped with 20 mM thulium 1,4,7,10-tetraazacyclododecane-1,4,7,10-tetrakis(methylene phosphonate) ($TmDOTP^{5-}$) (Macrocyclics) as the temperature dependencies of the exchangeable proton chemical shifts in TmDOTP are sensitive, linear, and well documented [19]. In particular, the H(6) proton provides a nicely resolved resonance for monitoring temperature changes. Because of its high ionic strength, the relatively small concentration of $TmDOTP^{5-}$ is expected to contribute significant rf loss. The sample rotation rate was regulated at 2 kHz, and bearing and drive air were supplied at room temperature. The sample temperature was regulated by means of an air stream cooled by a Bruker BCU-05 refrigeration unit and controlled by a BVT-3300. The rf heating experiment was run as follows: a presaturation pulse was applied to the probe for 40 ms at the test power level; this was followed by 5 ms of signal recovery before a standard pulse and acquire sequence. The duty cycle was maintained at a constant 3.8% while the presaturation power was varied. Before signal averaging, 256 dummy scans were run (taking ~5 min) in order for the sample to reach a steady state temperature.

The sample temperature rise due to rf irradiation can be seen in Fig. 4a. Even for the full rotor with 150 mM NaCl added to the

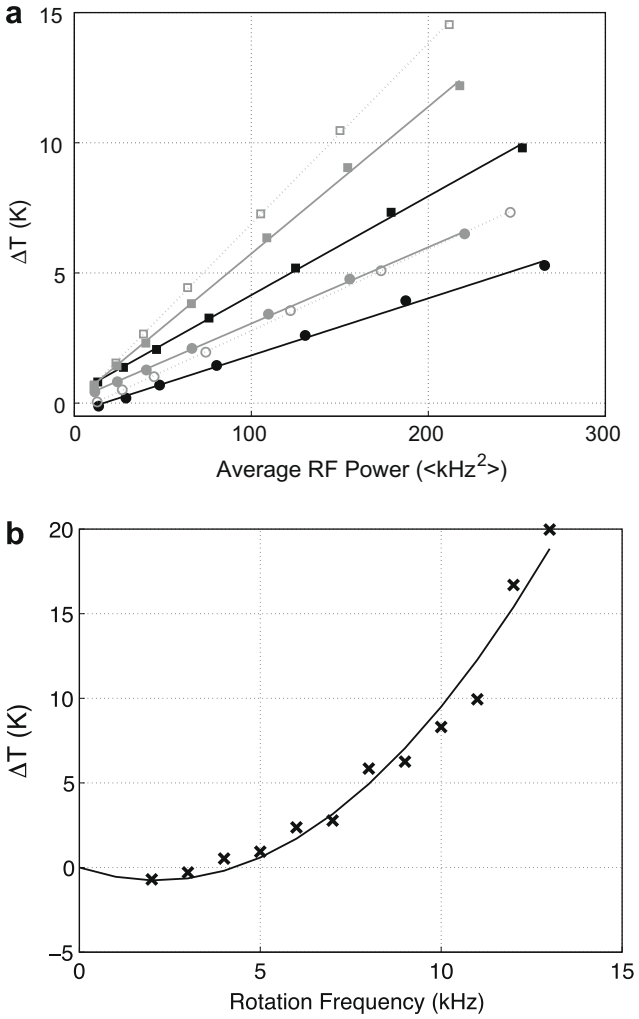

Fig. 4. (a) Average rf sample heating at three different sample lengths and two salt concentrations. Black filled circles: 20 mM $TmDOTP^{5-}$ with a 3.7 mm sample length. Black filled squares: 20 mM $TmDOTP^{5-}$ and 150 mM NaCl with a 3.7 mm sample length. Gray filled symbols correspond to the same solutions with a 6.7 mm sample length, and the empty symbols correspond to the same solutions with an 11.7 mm sample length. Lines are linear fits to the data as a visual guide. Note that because of its high ionic strength, small concentrations of $TmDOTP^{5-}$ still contribute significantly to rf loss. The rf heating remains under 15 K for all samples, and either decreasing the sample length or the salt concentration further reduces the heating. Average power was varied by keeping the duty cycle constant at 3.8% and varying the presaturation pulse power. A delay of 5 ms between the presaturation pulse and the acquire pulse was used and 256 dummy scans (~ 5 min) were run before acquiring to make sure the sample had reached equilibrium temperature. (b) Frictional heating due to MAS. The sample temperature was monitored using a sample containing 10% lead nitrate ($Pb(NO_3)_2$) diluted with NaCl to reduce its density. The gas lines were kept at room temperature. The line is a quadratic fit through the origin. The initial temperature drop is due to Joule-Thomson cooling. Heating at 13 kHz MAS reaches 20 K, which is enough to be a problem for biological samples, but it can be mitigated by cooling the rotor with chilled VT gas.

20 mM TmDOTP, the sample temperature increased less than 15 K. For the 20 mM TmDOTP samples, the heating was 7.4 K for a full-length sample (11.7 mm) at 246 kHz^2, 6.6 K for a 6.7 mm length sample at 220 kHz^2, and only 5.3 K for a 3.7 mm length sample at 266 kHz^2. From Fig. 4a we can see that the added 150 mM NaCl roughly doubles the amount of rf heating in the sample. The longer samples, which extend closer to the ends of the LGR coil where the *E* field is known to be higher [20], reached a somewhat higher temperature than the 3.7 mm samples. Further samples incorporating lipids (50 wt%) were also tested (data not shown), with results similar to those seen for samples without salt. The relatively low rf heating observed even with higher salt conditions demonstrates that the LGR reduces the conservative *E* field within the sample to an acceptable level that will neither damage the sample nor significantly affect NMR measurements. This is particularly critical for high field spectroscopy since the conservative *E* field scales linearly with B_0 for a fixed coil inductance and B_1 field [9]. The voltage across a coil, which determines the conservative *E* field, is proportional to the impedance of the coil, $\omega_0 L$, where ω_0 is the Larmor frequency.

The use of a low-inductance LGR for generation of ^{1}H rf fields has been shown to reduce rf heating in the sample by an order of magnitude during decoupling [9]. At the same time, our detection solenoid has multiple turns with an inductance much higher than the LGR. The strength of its conservative *E* field is mitigated by the lower Larmor frequency of ^{13}C. Also, the amount of time the ^{13}C channel is transmitting is typically less than half the time the ^{1}H channel is transmitting, since the ^{13}C channel is only transmitting during the excitation part of the experiment while ^{1}H decoupling is used during both excitation and acquisition. To be safe, it is prudent to compare amounts of heat generated in the sample by each of the coils. A simple way to estimate heating contributions from each rf channel under normal operating conditions is to use changes in a probe's *Q* or 90° pulse length when switching between lossy and non-lossy samples [7,9]. For the *Q* measurement, the amount of rf power dissipating in the dielectrically lossy sample for each kHz^2 of rf field can be written in W/kHz^2 as

$$q_{HEAT} = \left(\frac{Q_{NL}}{Q_{BIO}} - 1\right) \cdot \frac{1}{\eta_{NL}}, \quad (1)$$

where Q_{BIO} is the *Q* of a probe loaded with lossy (biological) sample and Q_{NL} and η_{NL} are the *Q* and power efficiency of a probe with a non-lossy reference. For our measurements, we used a 150 mM NaCl aqueous solution as a lossy sample. We chose water to serve as a non-lossy reference in order to maintain a similar dielectric constant and minimize re-tuning of the probe between the measurements of *Q*'s. Both samples occupied full volume of the rotor (11.7 mm in length). The *Q* values and calculated heat dissipation rates, q_{HEAT}, are listed in Table 1 for both ^{1}H and ^{13}C channels.

To compare amounts of ^{13}C and ^{1}H heating induced in the sample under typical operating conditions, we estimate heating during a typical windowless dipolar recoupling experiment, such as those described below. If the ^{1}H 93 kHz decoupling field is applied for 40 ms every second, the resulting heat dissipation is $0.91 \times (10^{-3}) \times 93^2 \times 0.04 = 0.31$ J into the sample per transient from the ^{1}H channel. The CP pulse and windowless excitation pulse train on the ^{13}C channel generally last half as long (20 ms) with rf fields held at 42.5 kHz, resulting in $5.0 \times 42.5^2 \times 0.02 = 0.18$ J of heat dissipated into the sample. Thus, with this probe design, the ^{13}C and ^{1}H channels contribute almost equal levels of heating in the sample under normal operation.

Table 1
Calculation of heat dissipation rates q_{HEAT}, per kHz^2 of rf field. *Q* values listed are at −3 dB. *Q* values were also measured at −7 dB to verify consistency.

Channel	Q_{NL}	Q_{BIO}	η_{NL} (kHz^2/W)	q_{HEAT} (mW/kHz^2)
^{1}H	147	141	46.7	0.91
^{13}C	119	90	64	5.0

3.2. Frictional heating

The aqueous samples used for measurement of rf heating will not spin reliably at high sample rotation rates, so powdered lead nitrate ($Pb(NO_3)_2$) samples were used to measure frictional heating due to sample rotation. The temperature dependence of the ^{207}Pb chemical shift (156.4 MHz at 17.6 T) is also well documented [21]. To reduce the density of the MAS sample to levels relevant to biological samples, lead nitrate was mixed with NaCl. Fine, ground crystals of NaCl were mechanically mixed with fine, ground crystals of lead nitrate to achieve a mixture that was ~10% lead nitrate by weight and to achieve a biologically relevant density of ~2.4 g/cm^3. Spectra were collected using a standard pulse-acquire sequence at different sample rotation rates while holding the VT gas temperature constant. A temperature equilibrium time of at least 10 min was used at each spinning speed. The full sample volume of a thick-walled rotor was used for these measurements.

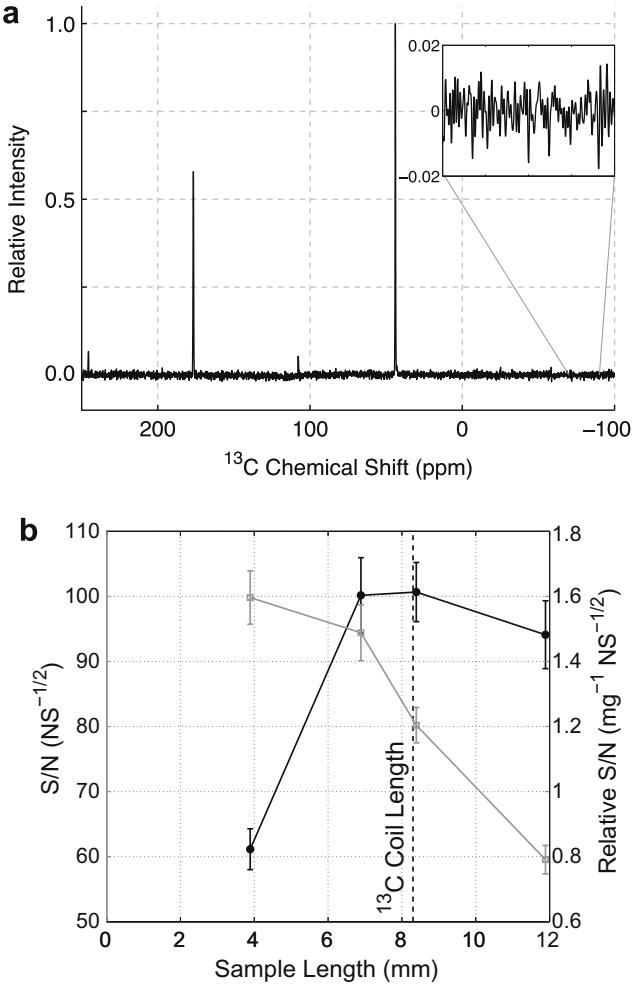

Fig. 5. (a) ^{NA}GLY ^{13}C CPMAS spectrum after 8 scans with a sample length of 6.9 mm containing 67.3 mg of glycine spinning at 13 kHz. Inset is a magnification of the noise used in the S/N measurement. This particular spectrum has a S/N measurement of 301. (b) S/N for ^{NA}GLY as a function of sample length. Shown are the S/N normalized for the number of scans (solid circles, left axis) as well as the S/N per unit mass (open squares, right axis), also normalized for the number of scans.

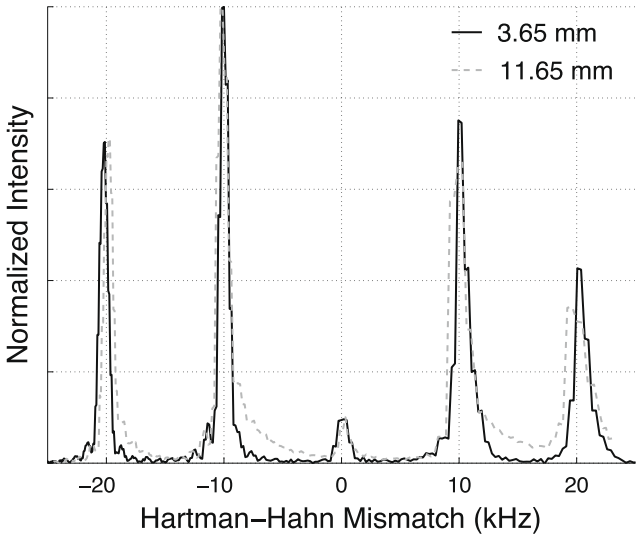

Fig. 6. CPMAS matching condition profile for adamantane at 10 kHz MAS using a square spinlock pulse on both rf channels. The ^{1}H rf field was held constant at $(\omega_1/2\pi) \sim 35$ kHz while the ^{13}C B_1 field was varied; the signal is graphed as a function of the rf mismatch. The solid line corresponds to a sample length of 3.7 mm; the dashed line corresponds to a sample length of 11.7 mm. The *X*-axis is the average ^{13}C B_1 field minus the average ^{1}H B_1 field. The longer sample (11.7 mm, dotted line) has broader, weaker matching conditions. This is from the wider range of rf energy the sample is exposed to due to the lower homogeneity of the ^{13}C B_1 field. The shorter sample (3.7 mm, solid line) shows excellent agreement with theory with maximal signal at mismatch levels equal to integer values of the spinning speed.

As shown in Fig. 4b, frictional sample heating was a maximum of 20 K when spinning at 13 kHz with a VT temperature of 298 K. It was noted that different bearing and drive pressures resulting in the same sample rotation rate cause varying levels of frictional heating.

4. Performance under normal operating conditions

4.1. Sensitivity measurements

Measurements of sensitivity were performed using crystalline, natural abundance glycine (α-form) to allow comparison to other published work. The veracity of this standard for determining true S/N is limited given that the quality of the spectra are determined by a number of interrelated factors. Measurements were done for the full sample length (11.9 mm) in a thin-walled rotor (95.6 μL sample volume) with a sample mass of 115.4 mg spinning at 13 kHz. Sample lengths of 8.4 mm with 83.6 mg of sample, 6.9 mm with 70.1 mg of sample, and 3.9 mm with 38.3 mg of sample were also examined. All spectra were collected at 13 kHz MAS. Signal was measured with a ramped cross-polarization sequence and 94 kHz SPINAL64 decoupling [22] during acquisition. A recycle delay of 30 s was used and signal was averaged over 1, 2, 4, and 8 scans with 2 dummy scans. Data (4096 points with a dwell of 10 μs) were Fourier transformed (without line broadening), phased, and signal was measured between 40–50 ppm for comparison to noise between −70 and −90 ppm (Fig. 5a).

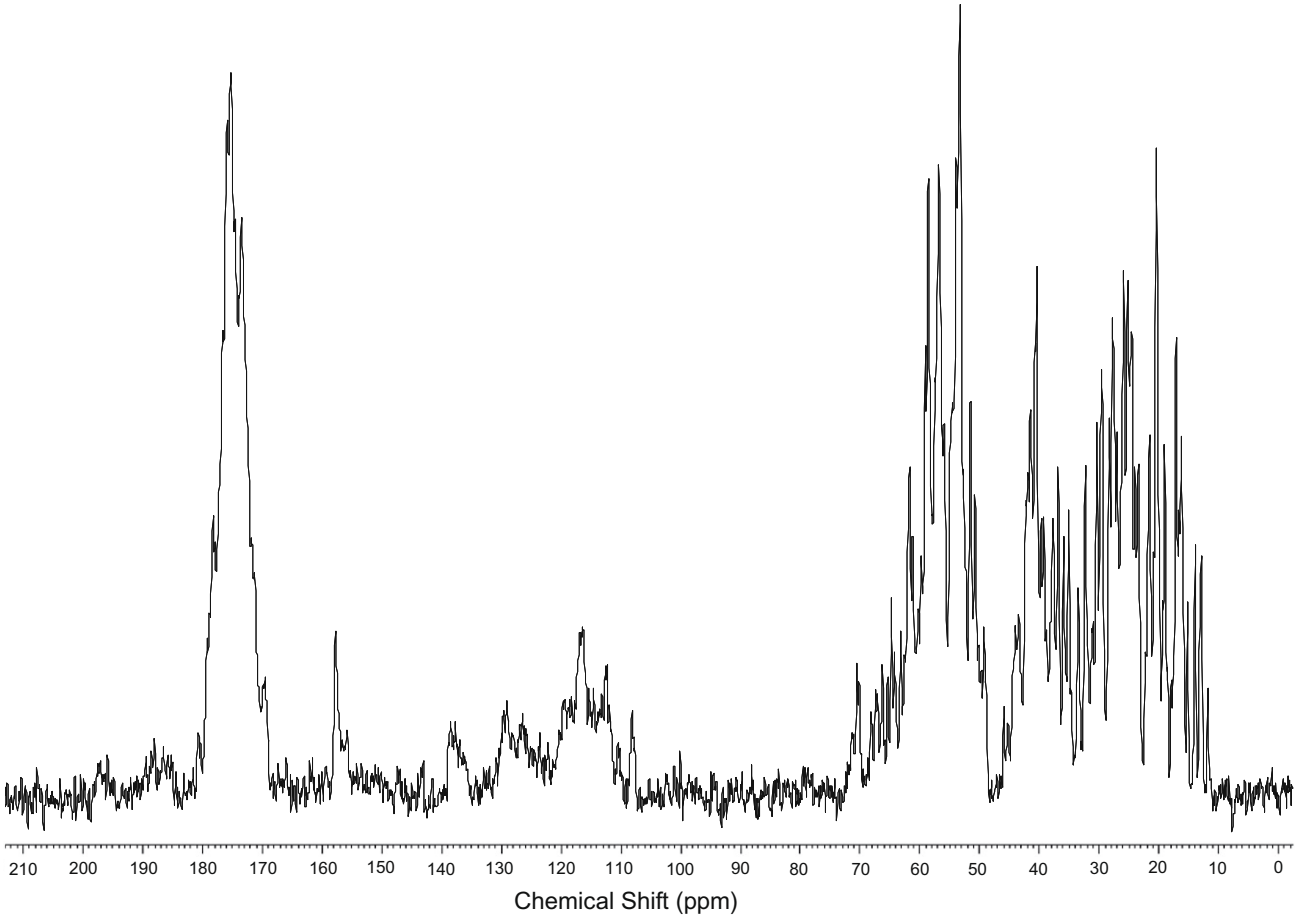

Fig. 7. ^{13}C CPMAS spectrum of nanocrystalline natural abundance lysozyme.

There are several formulae for calculating S/N. We have chosen a standard definition of S/N as being $P_H/(2 * N_{RMS})$, where P_H is signal peak height and N_{RMS} is the root-mean-square noise amplitude. The sensitivity of the probe was also characterized for a variety of sample lengths in order to allow quantitative determination of optimal conditions for applications in which one may be examining mass-limited samples or concentration-limited samples with either simple pulse sequences or pulse sequences requiring high B_1 and high homogeneity on the ^{13}C and/or ^{1}H channels for the best possible performance. For these measurements, the S/N is normalized to the square root of the number of scans, allowing S/N comparisons independent of the number of scans, as well as to the weight of the individual samples.

As can be seen in Fig. 5b, the best S/N per mg is with the smallest sample length and remains high for sample lengths less than 6.9 mm (83% of the coil length). The best overall S/N is achieved for samples lengths on the order of 6.9 mm and longer. The signal quality does not increase greatly once the sample length is on the order of or greater than the coil length (8.3 mm) and resolution is compromised for the longer samples.

For most applications that are concentration-limited rather than mass-limited, a sample geometry in which the rotor wall is the minimum thickness possible for a given spinning speed is optimal. A sample length on the order of 6.7 mm provides optimal S/N with acceptable rf homogeneity. Increasing the length of the sample beyond this point yields little in improving S/N and can even be detrimental to making quantitative measurements using standard ssNMR pulse sequences due to incomplete excitation of the full sample. For samples with limited quantities, the length of the sample can easily be adjusted using spacers allowing optimal S/N and rf performance.

4.2. Cross-polarization measurements

For static cross-polarization (CP), the best magnetization transfer is at the Hartmann–Hahn matching condition, which means that both nuclei are nutating at similar rates during the spin lock [23]. When optimizing CP on a MAS sample, the best transfer conditions are when the nutation rates differ by +/−1 or 2 times the MAS rate [24,25]. A CP profile can be generated by holding the rf field constant for one resonant frequency and varying the rf field for the other resonant frequency through these matching conditions. The symmetry and widths of the peak matching conditions as well as the overall profile reveal how homogeneous the B_1 fields are at the two frequencies and how well they overlap with respect to the sample [1]. CP matching profiles using square spin lock pulses were collected by fixing the ^{1}H power at $(\omega_1/2\pi) \sim 35$ kHz and varying the ^{13}C power (Fig. 6). Measurements were performed at a sample rotation rate of 10 kHz on adamantane samples that were 3.7 and 11.7 mm in length. The symmetry of the peaks indicates that the homogeneity and the overlap of the B_1 fields are quite good. For the longer sample the matching conditions become broader and less symmetric but are still considerably better than for multiply-resonant coils, particularly those that are not properly balanced [1]. This emphasizes the importance of homogeneity for efficient cross-polarization. The similarity of the measured profiles to an ideal profile is striking given that the two B_1 fields are generated by two orthogonal coils with different geometries.

4.3. Performance with a biologically relevant sample

To illustrate the performance of the Low-E MAS probe we collected a standard CPMAS spectrum on a microcrystalline protein.

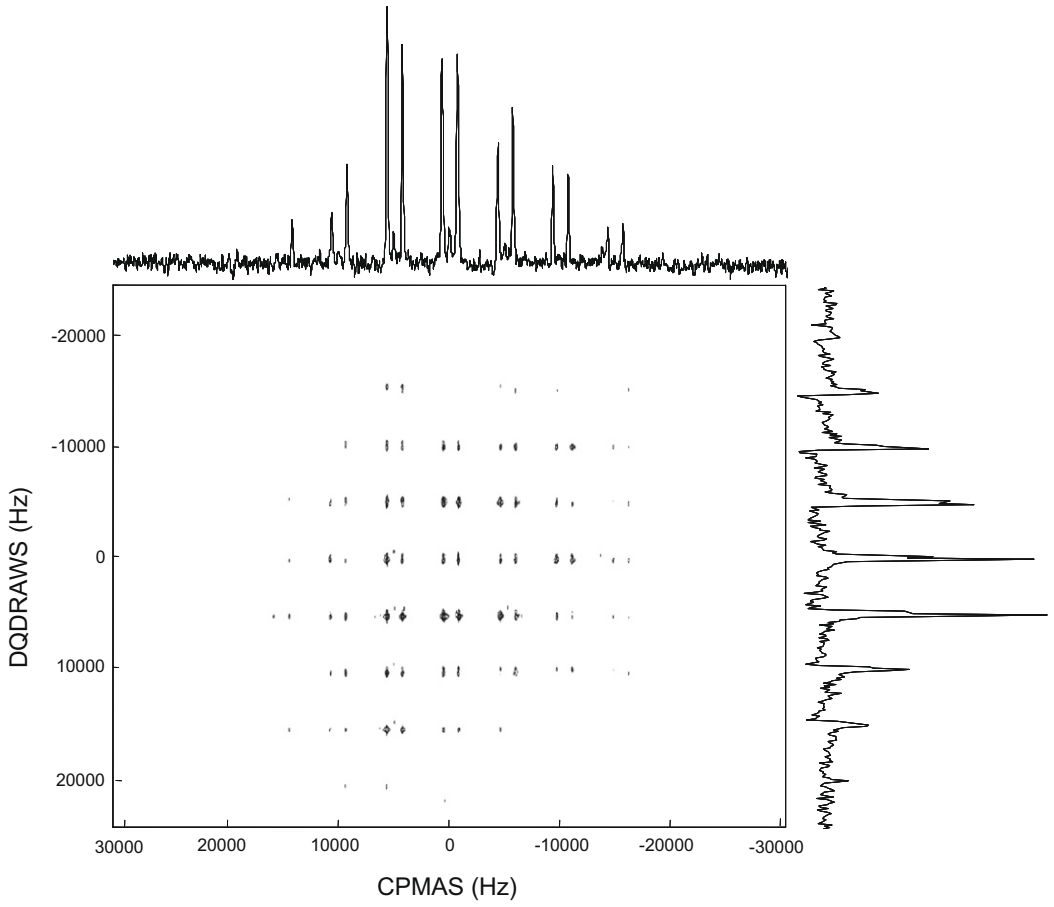

Fig. 8. A 2D DQ-CSA spectrum for *G*AV.

Lysozyme crystals were made by dissolving lysozyme at a concentration of ~50 mg/mL in deionized water. To this solution an equal volume of precipitation solution containing 3 M NaCl in 50 mM Tris buffer, pH 7.0 was added. The 1:1 mixture of protein solution and precipitation solution was left to evaporate at 40 °C for 2 days leading to crystal formation. The crystals were then collected by centrifugation and loaded into a rotor. A CPMAS spectrum (Fig. 7) verifies the crystallinity of the sample.

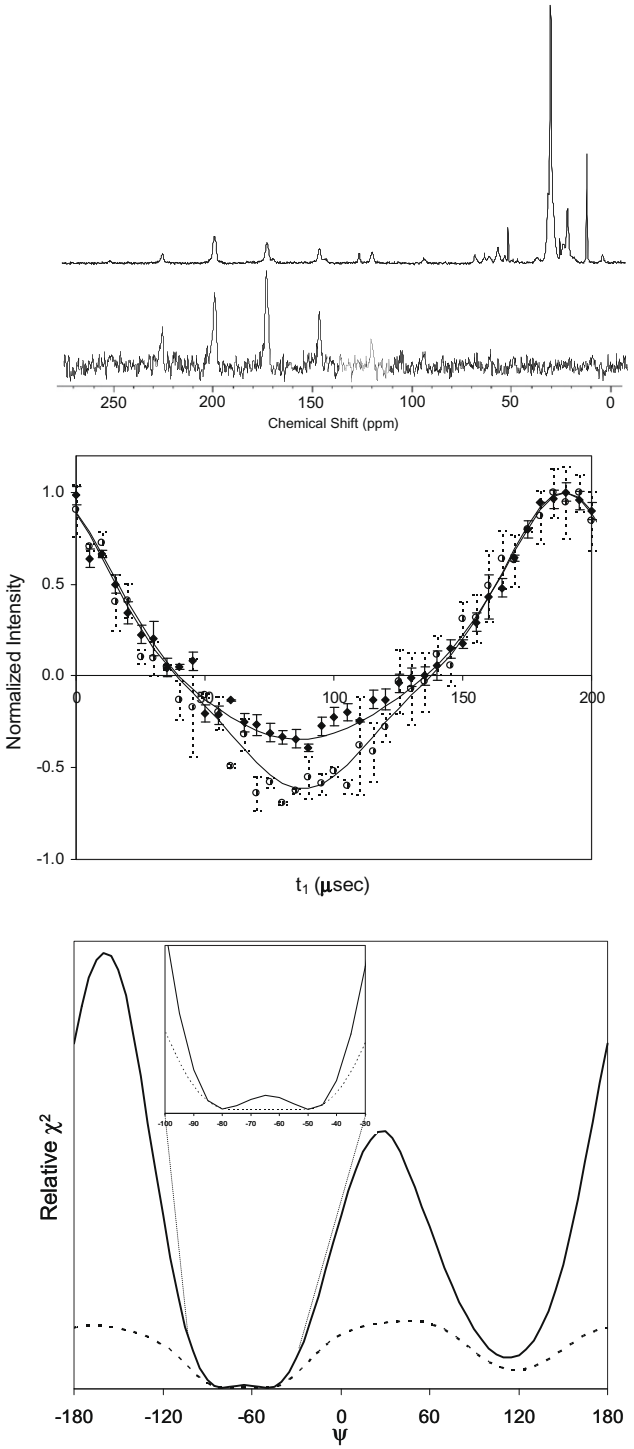

Fig. 9. (Top) CPMAS and DQ-filtered spectra for the 21 amino acid peptide KL_4 $^{13}C'$-enriched at positions L9 and L10 and incorporated into DPPC:POPG lipid vesicles at a peptide:lipid molar ratio > 1:50; the signals in the aliphatic region are primarily from the surrounding lipids. (middle) 2D DQ-CSA correlation data for the KL_4 sample along with best fit simulations. Closed and open symbols are data collected at 750 and 500 MHz, respectively; lines correspond to the signal trajectories for the best fit (ϕ,ψ) simulations at the two fields. (bottom) χ^2 evaluation of simulations with varying ψ while holding ϕ at a value obtained from DQ buildup experiments; solid and dashed lines correspond to fitting of data at 750 and 500 MHz, respectively. Note the improved selectivity of the χ^2 evaluation at 750 MHz due to the increased CSAs at the higher magnetic field.

4.4. Performance using mulipulse windowless rf sequences

DQDRAWS (Double Quantum Dipolar Recoupling in A Windowless Sequence) experiments [26] were performed on a tripeptide, $^{*}G^{*}AV$, which is $^{13}C'$ enriched on the first two amino acids (the enriched peptide is diluted to 10% with natural abundance peptide and crystallized). These experiments are useful at intermediate rotation rates (5–8 kHz) for determining torsion angles in peptides [27], yet, like many recoupling sequences, their performance is dependent on the availability of strong, homogeneous B_1 fields [28]. For these experiments, the CP contact time was 2.2 ms, cw decoupling was applied during the mixing period and SPINAL64 decoupling [16] was applied during acquisition. The MAS rate was 5 kHz, which corresponds to a $\pi/2$ pulse of 5.88 μs for the rotor-synchronized DRAWS sequence. Even with a full rotor (sample length 11.7 mm) and 5 kHz rotation rate (~104 kHz ^1H field and 42.5 KHz ^{13}C field) a DQ excitation efficiency of >25% was achieved for the enriched spins, which have a dipolar coupling of ~250 Hz. A 2D DQ-CSA spectrum was collected with a t_1 increment of 20 μs and evolution of 5.12 ms with 48 scans per slice and demonstrates the improved resolution of these experiments with high magnetic field (Fig. 8).

DQDRAWS data were also collected on a peptide in a lipid environment to demonstrate the utility of the low-E probe in examining protein structures under conditions in which the protein is inherently dilute. The sample consists of a 21-amino acid peptide (KL_4) isotopically enriched at two adjacent $^{13}C'$ positions and reconstituted in a lipid environment at a lipid:peptide molar ratio of >50:1. The sample was packed into a 6.7 mm length as this gave a reasonable filling factor for the amount of sample available. The DQ-filtered spectrum of this sample (Fig. 9) demonstrates the advantages of using a selection filter to simplify complicated spectra. The 2D DQ-CSA data validate the ability of this technique at high fields to isolate and characterize different peptide conformations if suitable rf fields are available without compromising the integrity of the sample. Fig. 9 also shows the improvements that can be had in fitting CSA-CSA correlation data by moving to a higher B_0 irrespective of the probes used due to the increased spans of the CSAs.

5. Conclusions

The low-E MAS probe was thoroughly characterized in order to determine the rf efficiency of each channel, maximum achievable B_1 fields, homogeneity of the B_1 fields, isolation between channels, stability at high power, rf-induced sample heating, frictional heating under MAS, spectral linewidths, and signal/noise on standard compounds. Under normal operating conditions, a ^1H rf field of $(\omega_1/2\pi) = 93$ kHz and homogeneity (810°/90°) of 95% can be obtained with a sample length of 8.4 mm and a sample volume of 68 μL. With a higher power amplifier, we should be able to exceed 110 kHz decoupling fields based on bench measurements. ^{13}C rf fields greater than $(\omega_1/2\pi) = 70$ kHz with homogeneity (810°/90°) of 70% are routinely observed for this sample length; the ^{13}C B_1 homogeneity can be increased to 89% with a 6.7 mm sample length. Under full ^1H decoupling for long periods of time, sample heating due to the strong rf fields is minimal even for samples containing physiological levels of salt. We have not noticed any sample degradation in heat sensitive samples after extensive experimentation. The power handling characteristics, B_1 fields, and homogeneities

make this an ideal probe for applying the full range of MAS solid state NMR experiments, including sequences which use extended periods of continuous rf pulsing on both channels, to biological samples which are inherently dilute.

Acknowledgements

We thank Prof. Arthur Edison, Dr. Douglas Elliott, Dr. Chunqi Qian, and Prof. Manish Mehta for helpful discussions in writing this paper. We thank Richard Desilets for careful fabrication of probe parts. We thank Katherine Sippel for help making the crystalline lysozyme. We thank the University of Florida High Performance Computing Center for the use of their cluster of computers for the numerical simulations. Funding was provided by NIH R01 HL076586, the National High Magnetic Field Laboratory in-house research program, and the University of Florida.

References

[1] E.K. Paulson, R.W. Martin, K.W. Zilm, Cross polarization, radio frequency field homogeneity, and circuit balancing in high field solid state NMR probes, J. Magn. Reson. 171 (2004) 314–323.
[2] P.L. Gor'kov, E.Y. Chekmenev, R.Q. Fu, J. Hu, T.A. Cross, M. Cotten, W.W. Brey, A large volume flat coil probe for oriented membrane proteins, J. Magn. Reson. 181 (2006) 9–20.
[3] R.W. Martin, E.K. Paulson, K.W. Zilm, Design of a triple resonance magic angle sample spinning probe for high field solid state nuclear magnetic resonance, Rev. Sci. Instrum. 74 (2003) 3045–3061.
[4] J.A. Stringer, C.E. Bronnimann, C.G. Mullen, D.H. Zhou, S.A. Stellfox, Y. Li, E.H. Williams, C.M. Rienstra, Reduction of RF-induced sample heating with a scroll coil resonator structure for solid-state NMR probes, J. Magn. Reson. 173 (2005) 40–48.
[5] J.B.D. de Lacaillerie, B. Jarry, O. Pascui, D. Reichert, "Cooking the sample": Radiofrequency induced heating during solid-state NMR experiments, Solid State NMR 28 (2005) 225–232.
[6] C.G. Li, Y.M. Mo, J. Hu, E. Chekmenev, C.L. Tian, F.P. Gao, R.Q. Fu, P.L. Gor'kov, W.W. Brey, T.A. Cross, Analysis of RF heating and sample stability in aligned static solid-state NMR spectroscopy, J. Magn. Reson. 180 (2006) 51–57.
[7] F.D. Doty, J. Kulkarni, C. Turner, G. Entzminger, A. Bielecki, Using a cross-coil to reduce RF heating by an order of magnitude in triple-resonance multinuclear MAS at high fields, J. Magn. Reson. 182 (2006) 239–253.
[8] S.V. Dvinskikh, K. Yamamoto, U.H.N. Durr, A. Ramamoorthy, Sensitivity and resolution enhancement in solid-state NMR spectroscopy of bicelles, J. Magn. Reson. 184 (2007) 228–235.
[9] P.L. Gor'kov, E.Y. Chekmenev, C.G. Li, M. Cotten, J.J. Buffy, N.J. Traaseth, G. Veglia, W.W. Brey, Using low-E resonators to reduce RF heating in biological samples for static solid-state NMR up to 900 MHz, J. Magn. Reson. 185 (2007) 77–93.
[10] B. Dillmann, K. Elbayed, H. Zeiger, M.C. Weingertner, M. Plotto, F. Engelke, A novel low-E field coil to minimize heating of biological samples in solid-state multinuclear NMR experiments, J. Magn. Reson. 187 (2007) 10–18.
[11] C.V. Grant, S.L. Sit, A.A. De Angelis, K.S. Khuong, C.H. Wu, L.A. Plesniak, S.J. Opella, An efficient $^{1}H/^{31}P$ double-resonance solid-state NMR probe that utilizes a scroll coil, J. Magn. Reson. 188 (2007) 279–284.
[12] P.L. Gor'kov, R. Witter, E.Y. Chekmenev, F. Nozirov, R. Fu, W.W. Brey, Low-E probe for $^{19}F-^{1}H$ NMR of dilute biological solids, J. Magn. Reson. 189 (2007) 182–189.
[13] A. Krahn, U. Priller, L. Emsley, F. Engelke, Resonator with reduced sample heating and increased homogeneity for solid-state NMR, J. Magn. Reson. 191 (2008) 78–92.
[14] A.A. De Angelis, S.J. Opella, Bicelle samples for solid-state NMR of membrane proteins, Nat. Protoc. 2 (2007) 2332–2338.
[15] S.C. Grant, L.A. Murphy, R.L. Magin, G. Friedman, Analysis of multilayer radio frequency microcoils for nuclear magnetic resonance spectroscopy, IEEE Trans. Magn. 37 (2001) 2989–2998.
[16] W. Froncisz, J.S. Hyde, The loop-gap resonator—a new microwave lumped circuit electron-spin-resonance sample structure, J. Magn. Reson. 47 (1982) 515–521.
[17] L.D. Hall, T. Marcus, C. Neale, B. Powell, J. Sallos, S.L. Talagala, A modified split-ring resonator probe for NMR imaging at high field strengths, J. Magn. Reson. 62 (1985) 525–528.
[18] S.A. McNeill, P.L. Gor'kov, J. Struppe, W.W. Brey, J.R. Long, Optimizing ssNMR experiments for dilute proteins in heterogeneous mixtures at high magnetic fields, Magn. Reson. Chem. 45 (2007) S209–S220.
[19] C.S. Zuo, K.R. Metz, Y. Sun, A.D. Sherry, NMR temperature measurements using a paramagnetic lanthanide complex, J. Magn. Reson. 133 (1998) 53–60.
[20] P.L. Gor'kov, C. Qian, J.A. Kitchen, M. Sharma, T.A. Cross, W.W. Brey, in: 49th Experimental Nuclear Magnetic Resonance Conference, Poster #012, Pacific Grove, CA, 2008.
[21] C. Dybowski, G. Neue, Solid state ^{207}Pb NMR spectroscopy, Prog. NMR Spec. 41 (2002) 153–170.
[22] B.M. Fung, A.K. Khitrin, K. Ermolaev, An improved broadband decoupling sequence for liquid crystals and solids, J. Magn. Reson. 142 (2000) 97–101.
[23] A. Pines, M.G. Gibby, J.S. Waugh, Proton-enhanced NMR of dilute spins in solids, J. Chem. Phys. 59 (1973) 569–590.
[24] E.O. Stejskal, J. Schaefer, J.S. Waugh, Magic-angle spinning and polarization transfer in proton-enhanced NMR, J. Magn. Reson. 28 (1977) 105–112.
[25] G. Metz, X.L. Wu, S.O. Smith, Ramped-amplitude cross-polarization in magic-angle-spinning NMR, J. Magn. Reson. A 110 (1994) 219–227.
[26] D.M. Gregory, M.A. Mehta, J.C. Shiels, G.P. Drobny, Determination of local structure in solid nucleic acids using double quantum nuclear magnetic resonance spectroscopy, J. Chem. Phys. 107 (1997) 28–42.
[27] M.A. Mehta, M.T. Eddy, S.A. McNeill, F.D. Mills, J.R. Long, Determination of peptide backbone torsion angles using double-quantum dipolar recoupling solid-state NMR spectroscopy, J. Am. Chem. Soc. 130 (2008) 2202–2212.
[28] T. Karlsson, J.M. Popham, J.R. Long, N. Oyler, G.P. Drobny, A study of homonuclear dipolar recoupling pulse sequences in solid-state nuclear magnetic resonance, J. Am. Chem. Soc. 125 (2003) 7394–7407.